The Astrophysical Journal, 714:852–859, 2010 May 1 doi:10.1088/0004-637X/714/1/852

THE ν_8 BENDING MODE OF DIACETYLENE: FROM LABORATORY SPECTROSCOPY TO THE DETECTION OF ^{13}C ISOTOPOLOGUES IN TITAN'S ATMOSPHERE

A. Jolly[1,6], A. Fayt[2], Y. Benilan[1], D. Jacquemart[3], C. A. Nixon[4,5], and D. E. Jennings[5]
[1] LISA, Université Paris 7 et 12, UMR 7583 du CNRS, 61 Avenue du Général de Gaulle, 94010 Créteil Cedex, France
[2] Laboratoire de Spectroscopie Moléculaire, Université Catholique de Louvain, Chemin du cyclotron 2, B-1348 Louvain-la-Neuve, Belgium
[3] LADIR, Université Paris 6, UMR 7075 du CNRS, Bat F 74,4 Place Jussieu, 75252 Paris 05, France
[4] Department of Astronomy, University of Maryland, College Park, MD 20742, USA
[5] NASA, Goddard Space Flight Center, Greenbelt, MD 20771, USA
Received 2009 December 22; accepted 2010 March 11; published 2010 April 15

ABSTRACT

The strong ν_8 band of diacetylene at 627.9 cm^{-1} has been investigated to improve the spectroscopic line data used to model the observations, particularly in Titan's atmosphere by *Cassini*/Composite Infrared Spectrometer. Spectra have first been recorded in the laboratory at 0.5 and 0.1 cm^{-1} resolution and temperature as low as 193 K. Previous analysis and line lists present in the GEISA database appeared to be insufficient to model the measured spectra in terms of intensity and hot band features. To improve the situation and in order to be able to take into account all rovibrational transitions with a non-negligible intensity, a global analysis of C_4H_2 has been carried out to improve the description of the energy levels up to $E_v = 1900$ cm^{-1}. The result is a new extensive line list which enables us to model very precisely the temperature variation as well as the numerous hot band features observed in the laboratory spectra. One additional feature, observed at 622.3 cm^{-1}, was assigned to the ν_6 mode of a ^{13}C isotopologue of diacetylene. The ν_8 bands of both ^{13}C isotopomers were also identified in the 0.1 cm^{-1} resolution spectrum. Finally, a $^{13}C/C_4H_2$ line list was added to the model for comparison with the observed spectra of Titan. We obtain a clear detection of ^{13}C monosubstituted diacetylene at 622.3 cm^{-1} and 627.5 cm^{-1} (blended ν_8 bands), deriving a mean $^{12}C/^{13}C$ isotopic ratio of 90 ± 8. This value agrees with the terrestrial (89.4, inorganic standard) and giant planet values (88 ± 7), but is only marginally consistent with the bulk carbon value in Titan's atmosphere, measured in CH_4 by Huygens GCMS to be 82 ± 1, indicating that isotopic fractionation during chemical processing may be occurring, as suggested for ethane formation.

Key words: astrochemistry – molecular data – planets and satellites: atmospheres – planets and satellites: detection

Online-only material: color figures

1. INTRODUCTION

Diacetylene was first identified in Titan's atmosphere in 1981 by the *Voyager* infrared interferometer spectrometer (IRIS; Kunde et al. 1981) and subsequently in the atmospheres of all four giant planets: Saturn in 1997 (de Graauw et al. 1997), Jupiter in 2004 (Kunde et al. 2004), Uranus in 2006 (Burgdorf et al. 2006), and Neptune in 2008 (Meadows et al. 2008). All detections were made in the infrared domain through the strong ν_8 perpendicular band at 627.9 cm^{-1}, while the weaker bending mode ν_9 at 220 cm^{-1} has only been detected in Titan (Kunde et al. 1981). Outside the solar system, diacetylene has been detected in two carbon-rich proto-planetary nebulae CRL 618 and CRL 2688 (Cernicharo et al. 2001). The molecule has even been detected outside the galaxy in the Large Magelanic cloud (Bernard-Salas et al. 2006). Each time, the detected band was ν_8 but the strong parallel band ν_6+ν_8 at 1241 cm^{-1} could also be identified (Cernicharo et al. 2001).

At the time of the first detection of C_4H_2, the fundamental vibration frequencies (see Table 1) were well established and the first rotational analyses of the ν_8 and ν_9 bands were available (Hardwick et al. 1979; Winther 1973). In contrast, accurate band intensity measurements were not available until 1984 (Koops et al. 1984). Laboratory experiments were thus performed by Kunde and colleagues to confirm the detection of diacetylene on Titan (Kunde et al. 1981). In particular, the observed intensity ratio of both detected bands could be verified using experimental spectra with a resolution similar to the infrared spectrometer IRIS on board *Voyager* (4.7 cm^{-1}). Kunde et al. (1981) could only obtain an estimation of the diacetylene mole fraction in Titan's atmosphere. Later, using a radiative transfer model and the measured band intensities (Koops et al. 1984), Coustenis et al. (1989) made the first determination of the abundance of diacetylene in Titan's atmosphere. The determinations of the mixing ratio of diacetylene were then improved (Coustenis & Bezard 1995) by using the results of a new rotational analysis of both ν_8 and ν_9 modes (Arié & Johns 1992). Using recorded spectra of C_4H_2 at high resolution (0.0014 cm^{-1}), Arié & Johns (1992) were able to identify and to analyze with great precision eight and four hot bands accompanying, respectively, the ν_8 and ν_9 fundamental bands. All the studied transitions arise from the first vibrational excited states ν_9 (220 cm^{-1}) and $2\nu_9$ (438 and 440 cm^{-1}). The analysis of hot bands is particularly important in the case of diacetylene because of their strong contribution even at low temperature. Calculations of the vibrational partition function show that between 100 and 200 K, which is the range of temperature sounded in Titan's, Jupiter's, and Saturn's atmospheres, the contribution of the hot bands is 10%–40% of the overall band intensity. By neglecting the hot bands in the analysis of the observations, those percentages are equivalent to the error made on the retrieved abundances. In addition, hot band features can be distinguished even at low spectral resolution. For example, the strongest hot band *Q* branch is seen at 626.85 cm^{-1}, one wavenumber away from the main band to the low energy side. While this feature is not distinguishable in the *Voyager* spectra due to low spectral resolution, it is clearly observed in

[6] Author to whom any correspondence should be addressed.

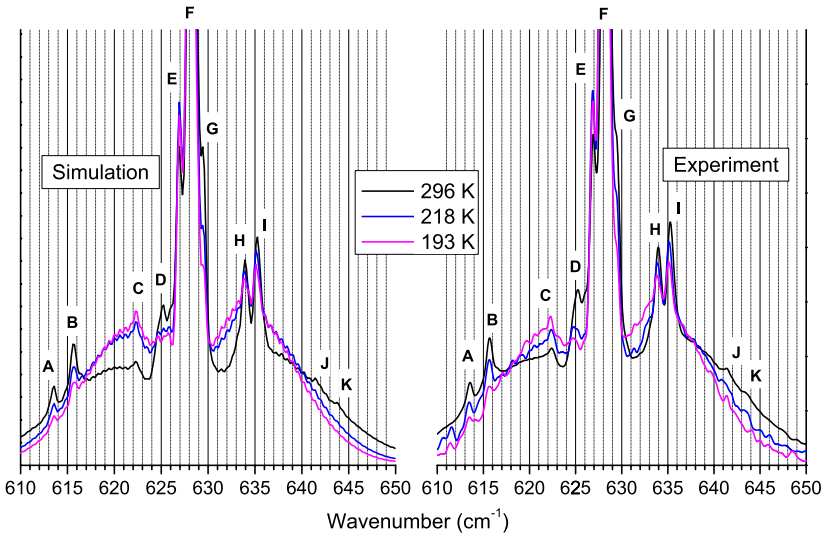

Figure 1. (Experiment) Temperature-dependent laboratory spectra of the ν_8 band of diacetylene taken at 0.5 cm^{-1} resolution (193, 218, and 296 K). The strong central band (F) has been truncated to help to distinguish the weaker hot band (A, B, D E, G, H, I, J, K) and isotopic features (C). (Simulation) Calculated spectra using the new line lists (C_4H_2 and ^{13}C–C_4H_2) presented in this paper.

(A color version of this figure is available in the online journal.)

Table 1
Fundamental Vibrational Frequencies for Diacetylene

Vibration	Frequency (cm^{-1})	Absolute Intensities (cm^{-2} atm^{-1}) at 296 K
ν_1 (σ_g^+)	3332.1541[a]	Not active
ν_2 (σ_g^+)	2188.9285[a]	Not active
ν_3 (σ_g^+)	871.9582[a]	Not active
ν_4 (σ_u^+)	3333.6647[a]	559.9[b]; 488[c]
ν_5 (σ_u^+)	2022.2415[a]	7.58[b]; 7.4[c]
ν_6 (π_g)	625.6436[a]	Not active
ν_7 (π_g)	482.7078[a]	Not active
ν_8 (π_u)	628.0409[a]	708.15[b]; 437[c]
ν_9 (π_u)	220.1236[a]	25.53[b]

Notes.
[a] Guelachvili et al. (1984).
[b] Koops et al. (1984).
[c] Khlifi et al. (1992).

the *Infrared Space Observatory* spectra (Coustenis et al. 2003) and also in the Composite Infrared Spectrometer (CIRS) spectra (Vinatier et al. 2007b) of diacetylene on Titan.

Unfortunately, neither Arié & Johns (1992) results nor the band intensity measurements (Koops et al. 1984) were included in the public GEISA database (Jacquinet-Husson et al. 2005). For the ν_8 region, GEISA included only the fundamental band. The total intensity for this band was equal to 4.10^{-18} cm^{-1} (molec $cm^{-2})^{-1}$ which is close to a factor of 2 smaller than the value that can be calculated for the fundamental band from the band intensity measurements (Koops et al. 1984). While some observers have used the GEISA data, others have used a more recent band intensity measurements (Khlifi et al. 1995) which also lead to errors. As can be seen in Table 1, the measured band intensity for ν_8 published by those authors is 1.6 times lower than Koops' value and undoubtedly in error due to saturation of the spectra (see Jolly & Benilan 2008). Khlifi's study of diacetylene is very similar to the study of cyanoacetylene (Khlifi et al. 1992), where intensity results for the strong bending modes of HC_3N were found to be in error due to saturation (Jolly et al. 2007). It is thus very likely that the ν_8 band intensity of diacetylene is also largely underestimated.

In this paper, we present the first low-temperature laboratory spectra of diacetylene and a new extensive analysis of the hot bands accompanying the ν_8 band. We focus on the numerous features that can be resolved at 0.5 cm^{-1} resolution including the contribution of the ^{13}C isotopologues of diacetylene. Finally, the new line list is used to improve the fit of the spectra of diacetylene taken by CIRS, allowing us to announce the first detection of the ^{13}C isotopologues of diacetylene in Titan's atmosphere.

2. EXPERIMENTAL RESULTS: LOW-TEMPERATURE SPECTRA

Spectra of diacetylene were recorded at three different temperatures (296, 218, and 193 K) and two different spectral resolutions (0.1 and 0.5 cm^{-1}). Low-temperature spectra were obtained with the Bruker IFS 120 HR interferometer in Paris (LADIR laboratory). The interferometer was equipped with a Ge/KBr beam splitter, an MCT photovoltaic detector, and a Globar source. To reach the low temperatures, the cell was first filled with C_4H_2 and N_2 at room temperature, and then cooled using methylcyclohexane and liquid nitrogen. For all spectra the whole optical path was under vacuum. A multipass cell of 100 cm base length was used for a total absorption path of 415 cm. The cell was equipped with KCl windows. The temperature of the gas inside the cell was recorded with four platinum probes at different places in the cell. A maximum difference of ±3K between the four probes was observed at 193 K. Because the probes were not in the center of the cell where the beam is going through, the temperature of the absorbing gas is probably underestimated by 1–5 K. The minimum experimental temperature of 193 K is due to the rapidly diminishing vapor pressure.

In addition, room temperature spectra have also been recorded in Creteil using a Brucker Equinox 55 FTIR spectrometer with the same apparatus used for the cyanoacetylene study (Jolly et al. 2007).

Spectra taken at three different temperatures at 0.5 cm^{-1} resolution with 1 atm of N_2 added to the sample are shown in Figure 1 (experiment). All observed Q branches are referred with a capital letter (A–K), also used later in other figures and

tables. Strong absorptions of the main Q branch (F) were cut out in the figure to concentrate on the hot band features. As mentioned above, the predicted hot band feature at 626.85 cm^{-1} (E) is clearly resolved from the main band. Surprisingly, many other hot band features are observed at 613.50 (A), 615.65 (B), 625.18 (D), 633.84 (H), and 635.25 (I) cm^{-1}. A strong feature appearing as a shoulder of the main Q branch at 629.45 cm^{-1} (G) is also observed. Note that those bands have never been studied since previous analysis (Arié & Johns 1992) was restricted to the strongest hot bands with Q branches in the range between 626.5 and 629 cm^{-1}. As expected, the intensity of the hot bands decreases at lower temperature but all those hot band features are still clearly visible at 193 K. The hot band at 626.85 cm^{-1} (E) is an exception since it increases when the temperature decreases to 218 K and is still strong at 193 K. This behavior is in fact, completely in agreement with the assignment of this feature to a hot band starting from ν_9 (220 cm^{-1}). Indeed, the Boltzmann population at 220 cm^{-1} increases by 20% when the temperature cools from 296 to 218 K and then decreases by only 2% between 218 and 193 K. The E Q-branch intensity follows very nicely this population variation. The population distribution can also be observed on the shape of the P and R branches which get narrower at lower temperature inducing an increase of intensity closer to the center of the band and a fast decrease further from the center.

Close to the top of the P branch in the cold spectra, at 622.26 cm^{-1} (C), a small feature is observed that cannot be assigned to a hot band since it does not decrease with decreasing temperature. As will be shown later, this feature is due to a ^{13}C isotopologue of diacetylene. On the high frequency side, two small features are observed at 641.40 (J) and 643.70 (K) cm^{-1}, only in the room temperature spectrum.

3. GLOBAL ANALYSIS BASED ON HIGH-RESOLUTION SPECTRA

In their high-resolution analysis of the ν_8-band complex (Arié & Johns 1992), Arié & Johns were able to analyze nine bands (18 subbands counting e and f symmetries separately), from the ground state and excited states ν_9 (220 cm^{-1}) and $2\nu_9$ (440 cm^{-1}). To extend this study, we have used the list of wavenumbers and intensities of their original spectra, kindly transmitted by Eric Arié, but rather few new bands were obtained because of the lack of information about both lower and upper states of the next hot bands.

On the basis of our experience in global rovibrational analyses of linear carbon chain molecules, more particularly C_2H_2 (Amyay et al. 2009), C_4N_2 (Fayt et al. 2004, Winther et al. 2005), and HC_3N (Fayt et al. 2008), we decided to develop the global analysis of C_4H_2. Recently, a similar study has been carried out on the bending modes of HC_3N (Jolly et al. 2007) and eventually led to the detection of ^{13}C isotopologue of HC_3N on Titan (Jennings et al. 2008). In such global analyses, we take into account simultaneously all resonance terms: anharmonic resonances, vibrational and rotational ℓ-type resonances, and Coriolis resonances. In a single-weighted least-squares procedure, we fit all observed rotational and rovibrational transitions, and we determine a single set of molecular parameters instead of numerous sets of state or band parameters.

In addition to Arié's spectra (the ν_9- and ν_8-band systems), the main source of high accuracy data was the extensive study in the 1850–3584 cm^{-1} range by Guelachvili et al. (1984), including data about high energy combinations of the ν_6 and ν_8 modes, and complementary informations about the low-energy gerade states ν_7 (483 cm^{-1}), ν_6 (625 cm^{-1}), and ν_3 (872 cm^{-1}). The $\nu_6 + \nu_8$ band (1241 cm^{-1}) has been studied by Matsumura et al. (1986), with indirect informations about the $2\nu_8$ and $2\nu_6$ states. In the microwave spectral domain, Matsumura and coworkers have observed and fully analyzed the $\nu_8 - \nu_6$ (Matsumura et al. 1981) and the $\nu_8 + \nu_9 - \nu_6 - \nu_9$ (Matsumura & Tanaka 1982) bands.

Step by step, using predictions (both in frequency and in intensity) based on the global analysis, many new subbands were identified in Arié's spectra and introduced in the data set, improving the quality of the global analysis leading to more and more parameters. Those spectra have finally been fully assigned: more than 50 subbands. Nevertheless, for such a six atom molecule with five stretching modes and four degenerate bending modes, the number of molecular parameters is quite high, and many important parameters were not yet determined by lack of experimental data. Veli-Matti Horneman (Oulu) kindly agreed to synthesize the diacetylene molecule and to record and measure its high-resolution infrared spectrum from 672 to 2110 cm^{-1}. With pathlengths of 48 or 163 m, a near-Doppler resolution, and an 0.0001 cm^{-1} accuracy, those spectra give access to an impressive number of bands reaching most substates of C_4H_2 up to more than 2000 cm^{-1}, combinations of the low-energy modes $\nu_3(\sigma_u^+)$, $\nu_6(\pi_g)$, $\nu_7(\pi_g)$, $\nu_8(\pi_u)$, and $\nu_9(\pi_u)$. All assignments (about 400 subbands) were introduced in the global analysis, providing a coherent set of more than 400 molecular parameters. This work is in progress and will be published separately (A. Fayt et al. 2010, in preparation).

4. Q BRANCHES IN THE LOW-RESOLUTION SPECTRA

On the basis of the molecular parameters determined by the global analysis, we were able to generate automatically a calculated spectrum of the ν_8-band complex, with a single transition dipole moment ($\Delta\nu_8 = +1$). Details about this procedure can be found in two papers (Fayt et al. 2004, Winther et al. 2005) devoted to C_4N_2 spectra. Our Hamiltonian includes all kinds of vibrational and rotational resonances which heavily mix most substates, so that the agreement between calculated and observed intensities is good in all cases. Absolute intensities for all lines were then obtained by scaling the sum of the intensities of all lines to the integrated band intensity measured by Koops et al. (1984; 2.86×10^{-17} cm^{-1} (molec $cm^{-2})^{-1}$ or 708 cm^{-2} atm^{-1}). For the wavenumbers, the accuracy is between 0.0001 and 0.001 cm^{-1} for transitions to observed substates. For most other transitions (very weak hot bands), we estimate that the accuracy is between 0.001 and 0.1 cm^{-1}.

Using the new line list, we were able to calculate spectra at all temperatures. Figure 1 (simulation) shows synthetic spectra comparing very well with our experimental spectra in terms of temperature variations and Q-branch features.

We will now focus on the bands with Q branches distinguishable at room temperature with a resolution of 0.5 cm^{-1}, referenced by capital letters A–L in Figure 1. In Table 2, we give their observed band maximum with an accuracy close to 0.05 cm^{-1}, their main assignment(s), their band origin(s) deduced from the global analysis with an accuracy better than 0.001 cm^{-1}, and finally an estimated relative intensity obtained by scaling the calculated intensity of the strongest line of the Q branch for each band to a maximum of 100 for the fundamental band.

Figure 2 presents the contribution of hot bands to the overall intensity as a function of the maximum energy E'' of the lower vibrational states we consider. The curve with the least

Table 2
Summary of the Diacetylene Q Branches Distinguishable at Room Temperature with a Resolution of 0.5 cm^{-1}

Q Branch	Maximum (cm^{-1})	Upper State	Lower State	Origin (cm^{-1})	Relative Intensity
A	613.50	$2\nu_6$ ($\Sigma\, e$)	ν_8 ($\Pi\, f$)	613.424	1.4
B	615.65	$\nu_6+\nu_8$ ($\Sigma\, e$)	ν_6 ($\Pi\, f$)	615.564	2.3
C[a]	622.26	ν_6 ($\Pi\, f$)	GS ($\Sigma\, e$)	622.198	0.5
D	625.18	$\nu_6+\nu_8$ ($\Sigma\, f$)	ν_6 ($\Pi\, e$)	625.079	2.4
E	626.85	$\nu_8+\nu_9$ ($\Sigma\, e$)	ν_9 ($\Pi\, f$)	626.846	14.7
F	628.0	ν_8 ($\Pi\, f$)	GS ($\Sigma\, e$)	627.894	100.0
G	629.45	$2\nu_8$ ($\Sigma\, e$)	ν_8 ($\Pi\, f$)	629.484	3.3
		$\nu_7+\nu_8$ ($\Sigma\, e$)	ν_7 ($\Pi\, f$)	629.530	5.3
H	633.84	$\nu_6+\nu_8$ ($\Delta\, e,f$)	ν_6 ($\Pi\, f,e$)	633.750	2×2.4
I	635.25	$2\nu_8$ ($\Delta\, e,f$)	ν_8 ($\Pi\, f,e$)	635.056	2×3.5
J	641.40	$3\nu_8$ ($\Phi\, e,f$)	$2\nu_8$ ($\Delta\, f,e$)	641.391	2×0.24
K	643.70	$\nu_6+2\nu_8$ ($\Phi\, e,f$)	$\nu_6+\nu_8$ ($\Delta\, f,e$)	643.677	2×0.16
L	651.7	ν_3 ($\Sigma\, e$)	ν_9 ($\Pi\, f$)	651.984	0.6

Note. [a] $H^{13}CCCCH$.

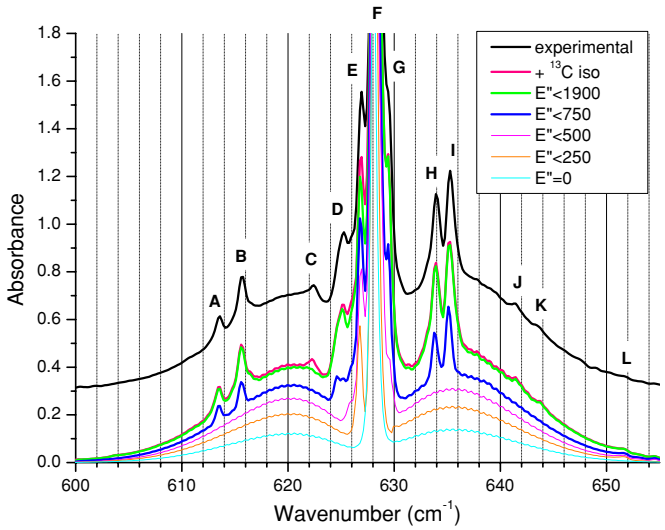

Figure 2. Experimental spectra of the ν_8 band of diacetylene taken at 0.5 cm^{-1} resolution and 296 K compared to calculated spectra taking into account transitions arising from the ground vibrational states ($E'' = 0$) and progressively higher lying excited states ($E'' < 250$, 500, 750, 1900 cm^{-1}) and finally the contribution of the ^{13}C istopologs of diacetylene. The strong central band was truncated and the experimental spectrum was shifted by 0.3 for clarity.

(A color version of this figure is available in the online journal.)

absorbance in the graph ($E'' = 0$) corresponds to the fundamental band (F) and is comparable to what was available in the GEISA database. In the following curves ($E'' < 250$ and $E'' < 500\,cm^{-1}$), we also consider the hot bands starting from ν_9 and from $2\nu_9$ and ν_7 (482 cm^{-1}), respectively. As already mentioned, the strongest hot band Q branch (E) at 626.85 cm^{-1} is mainly due to a hot band from the ν_9 state, but transitions from $2\nu_9$ also add intensity to this strong feature. One hot band from the ν_7 state contributes to the shoulder (G) centered at 629.5 cm^{-1}.

In the next curve (E″ < 750 cm^{-1}), we add numerous hot bands starting from ν_6 (625 cm^{-1}), ν_8 (628 cm^{-1}), $3\nu_9$ (657–661 cm^{-1}), and $\nu_7+\nu_9$ (701–702 cm^{-1}). As it is the case for many hot bands, the Q branches of the transitions from $3\nu_9$ and $\nu_7 + \nu_9$ are overlapped by stronger features in the central part of the complex. On the contrary, hot bands from ν_6 and ν_8 are broadly spread, a result of the strong anharmonicity of the combination of those two modes, also responsible for the high intensity of the $\nu_6+\nu_8$ combination band at 1241 cm^{-1}. The hot bands from ν_6 reach the $\nu_6+\nu_8$ state, with its four Σ^e, Σ^f, Δ^e, and Δ^f substates. The large positive value of the diagonal anharmonic parameter $x_{\ell_6\ell_8}$ shifts the Δ and Σ substates by about 7 cm^{-1} up and down, respectively. The large negative value of the vibrational ℓ-type resonance parameter r_{68} shifts the Σ^e and Σ^f substates by about 5 cm^{-1} down and up, respectively. So the hot bands from ν_6 are the main contributions to the B (615.65 cm^{-1}), D (625.18 cm^{-1}) and H (633.84 cm^{-1}) Q branches, with the upper substates $\nu_6+\nu_8$ Σ^e, Σ^f, and $\Delta^{e,f}$, respectively. The hot bands from ν_8 reach the $2\nu_8$ Σ or Δ substates. The anharmonic interaction associated with the k_{6688} anharmonic potential term shifts the close lying $2\nu_8$ and $2\nu_6$ substates by about 4 cm^{-1} up and down, respectively. So the hot bands from ν_8 to $2\nu_8$ appear on the high wavenumber side of the spectrum, the features G (629.45 cm^{-1}) and I (635.25 cm^{-1}) for the upper substates Σ and Δ, respectively. Another consequence of this anharmonic resonance is a heavy mixing of the $2\nu_8$ and $2\nu_6$ substates so that about 30% of the $2\nu_8$–ν_8 intensity is transferred to the $2\nu_6$–ν_8 band which was expected to be of negligible intensity (three quanta transition). Those subbands appear on the low wavenumber side of the spectrum, the nice Q-branch A (613.50 cm^{-1}) for $2\nu_6\Sigma$ –ν_8 and the left shoulder of the feature D (625.18 cm^{-1}) for $2\nu_6\Delta$ –ν_8.

Although all important features of the spectrum at room temperature and 0.5 cm^{-1} resolution are now explained by considering lower states up to 750 cm^{-1}, hot bands from higher energy states are far from negligible in terms of intensity. Dividing the energy scale from 0 to 2000 cm^{-1} in eight parts of 250 cm^{-1}, the number of vibrational substates into each interval is 3, 5, 12, 23, 44, 97, 186, and 306, respectively. This almost exponential increase of the number of substates according to the energy partly compensates the exponential decrease of their population according to the Boltzmann law. By adding hot bands up to $E'' = 1900$ cm^{-1} the overall intensity of the band is still enhanced by 22% as can be calculated by summing the intensity of the lines. Figure 2 also shows this final synthetic spectrum ($E'' < 1900$ cm^{-1}) which compares very nicely with the experimental one which is shifted up by 0.3 for clarity. The D feature appears quite stronger, and the very weak J (641.40 cm^{-1}) and K (643.70 cm^{-1}) Q branches now appear in the calculated spectrum. They are assigned to the $3\nu_8\Phi - 2\nu_8\Delta$ and $(2\nu_6 + \nu_8)\Phi - (\nu_6+\nu_8)\Delta$ bands, respectively. The weak Q branch C (622.26 cm^{-1}) remains unassigned because it is due to a ^{13}C isotopomer of diacetylene. The ^{13}C species are the subject of the next chapter, and the introduction of their contributions in the synthetic spectrum still improves the agreement with the

Table 3
Summary of the Analysis of the ν_6 and ν_8 Bands of $H^{13}CCCCH$ and $HC^{13}CCCH$

Band origin for HCCCCH	ν_6 : 625.497		ν_8 : 627.894	
	$H^{13}CCCCH$	$HC^{13}CCCH$	$H^{13}CCCCH$	$HC^{13}CCCH$
Predicted shift (Simmonet et al.)	−3.3	0.0	−0.9	−0.3
Predicted band origin	622.2	**625.5**	627.0	627.6
Band maximum in 0.1 cm^{-1} resolution spectra	622.26(1)	Not observed	627.02(1)	627.62(1)
Band origin from 0.1 cm^{-1} resolution spectra	**622.20(1)**	...	626.96(1)	627.56(1)
Band origin from 0.0014 cm^{-1} resolution spectra	...	...	**626.962(1)**	**627.558(1)**
Relative intensity (100 for ν_8 of HCCCCH)	23(6)	< 5	65(12)	100(15)

Notes. All values, but intensities, are in cm^{-1}. The best values are in bold. Estimated uncertainties (1σ) are given in parentheses in units of the last digit quoted.

experimental spectrum. A last remark about Figure 2: just under 652 cm^{-1}, the just visible Q-branch L (651.7 cm^{-1}) is broadly spread to the low frequency side and has been assigned to the $\nu_3 - \nu_9$ band. Its intensity results from the light mixing of ν_3 and $\nu_8+\nu_9$ Σ states due to the anharmonic resonance associated with the k_{389} anharmonic potential parameter.

Relative intensities were finally calculated for all allowed transitions with $\Delta\nu_8 = +1$ and $E'' < 1900$ cm^{-1}. A list of lines with their position and relative intensities is generated by choosing a very low minimum intensity threshold (0.003 on a scale where the strongest line in the cold band Q branch has an intensity of 100) to ensure that no intensity contribution is neglected. This new line list for ν_8 together with a new line list of the ν_9 band also based on the present study is available in the latest version of the GEISA database. Details about the line list will be presented in a forthcoming publication (N. Jacquinet-Husson et al. 2010, in preparation).

5. ^{13}C ISOTOPOLOGUES IN THE LABORATORY

The quality of the CIRS data currently retrieved by the *CASSINI* spacecraft on Titan has made possible the detection of a large number of isotopologues. It includes deuterated molecules such as C_2HD (Coustenis et al. 2008) as well as ^{18}O and ^{15}N bearing molecules such as $CO^{18}O$ (Nixon et al. 2008b) and $HC^{15}N$ (Vinatier et al. 2007a), but most of the detected isotopologues are ^{13}C bearing molecules. Many recent papers describe the detection via infrared spectroscopy of such molecules: $H^{13}CN$ (Vinatier et al. 2007a), $^{13}CH_3D$ (Bezard et al. 2007), $^{13}CH_4$, $H^{13}CCH$, $H_3{}^{13}CCH_3$ (Nixon et al. 2008a), $H^{13}CCCN$ (Jennings et al. 2008) and $^{13}CO_2$ (Nixon et al. 2008b). Concerning diacetylene, the absence of spectroscopic data about the ^{13}C isotopologues was preventing the search for those species. It is one of the goals of this study to obtain the needed spectroscopic parameters.

The positions of the ν_8 band of monosubstituted ^{13}C isotopomers were not known from any experimental study. Tay et al. (1995) have reported the only spectroscopic work performed with enriched samples. They have analyzed a large number of diacetylene isotopologues but unfortunately the studied region between 3100 and 3600 cm^{-1} does not include the bending modes. Calculations of isotopic shifts by Botschwina (1982) were also restricted to the stretching modes. In our laboratory spectra obtained at 0.5 cm^{-1} resolution with standard isotopic abundances (Figure 1), only one feature could be assigned to a ^{13}C isotopomer, the Q branch at 622.26 cm^{-1} (C). The problem was that this intensity was too low by a factor of 4 compared to the expected intensity of the ν_8 band of a ^{13}C isotopologue with a standard abundance. The solution came from the very recent isotopic shifts calculations by Simmonett et al. (2009). As summarized in Table 3, the positions for the ν_8 bands of $H^{13}CCCCH$ and $HC^{13}CCCH$ were predicted to be very close to the ν_8 fundamental band of C_4H_2 shifted by only −0.9 and −0.3 cm^{-1}, respectively. Compatible with the difficulty of detecting those species at low resolution, those values also excluded the Q branch at 622.26 cm^{-1}. This mysterious feature was finally assigned to the ν_6 band of $H^{13}CCCCH$. Monosubstituted diacetylenes are no longer symmetric, with the result that the gerade/ungerade symmetry character disappears, allowing symmetric bending modes such as ν_6 to gain some intensity. The band centers of the ν_6 bands of $H^{13}CCCCH$ and $HC^{13}CCCH$ were predicted by Simmonett et al. (2009) to lie at 622.2 and 625.5 cm^{-1}, respectively, the first one obviously corresponding to the feature C and the second one unobservable in the crowded central region between the D and E features.

We then started the global analysis of the two ^{13}C species, with all parameters fixed according to their normal species value, except the B_0 ground-state rotational constants determined by Tay et al. (1995) and the band centers corrected by the isotopic shifts predicted by Simmonett et al. (2009). The spectra of the cold and first hot bands of both ^{13}C species were calculated including the ^{13}C line list into the synthetic spectrum (Figure 2). The feature C (622.3 cm^{-1}) was very well reproduced assuming a quarter of the intensity of the ν_8 bands for the ν_6 bands. The agreement was also improved close to the strong hot band feature E near 627 cm^{-1}, thanks to the contribution of the two ν_8 bands.

Figure 3 shows the portion of spectra of interest for isotopic bands recorded at 0.1 cm^{-1} resolution. The plot of the difference (exp. − calc. without ^{13}C) makes evident the Q branches of the ν_8 band of $H^{13}CCCCH$ (627.02 cm^{-1}) and $HC^{13}CCCH$ (627.62 cm^{-1}), and of the ν_6 band of $H^{13}CCCCH$ (622.26 cm^{-1}), in perfect agreement with the ab initio predictions (Simmonett et al. 2009). On the other hand, the ν_6 band of $HC^{13}CCCH$, predicted at 625.5 cm^{-1}, is not clearly observed in this spectrum. Also, the ν_8 band of $H^{13}CCCCH$ appears weaker than the ν_8 band of $HC^{13}CCCH$. On the basis of those values, we were able to identify in Arié's high-resolution spectra the ν_8 band of the two ^{13}C species, at the limit of the noise, reaching so an accuracy of 0.001 cm^{-1}.

All those results are summarized in Table 3 where the last line presents the estimated relative intensities which yield the best agreement in the plot of the difference (experimental − calculated with ^{13}C) in Figure 3. Both isotopomers seem to have different behaviors concerning the band intensities of ν_6 and ν_8. Both CH bending modes are logically more influenced by an

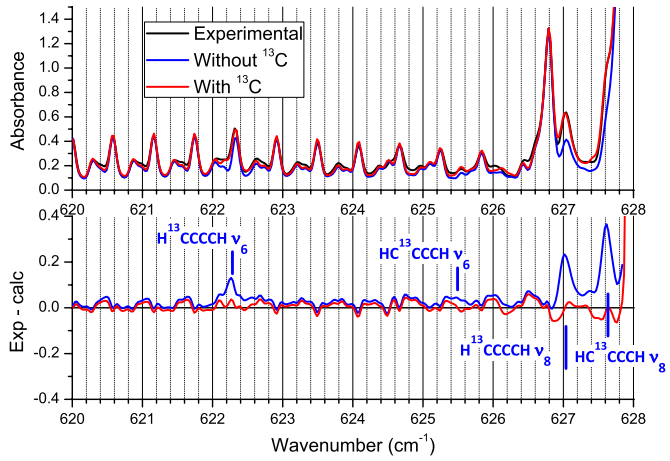

Figure 3. Upper: experimental spectra of the ν_8 band of diacetylene taken at 0.1 cm^{-1} resolution and 193 K compared to calculated spectra with and without the contribution of ^{13}C isotopologues of C_4H_2. Lower: subtraction between the experimental spectrum and the calculated spectra presented in the upper panel. Indicated positions of ν_6 and ν_8 for both isotopomers of C_4H_2 are those predicted by Simmonett et al. (2009).

(A color version of this figure is available in the online journal.)

external position of the ^{13}C than by a central position so that the isotopic shifts are larger for H^{13}CCCCH than for HC^{13}CCCH. The effect of the external position of the ^{13}C on the intensities seems to enhance the ν_6 band and to diminish the ν_8 band, while the central position does not seem to change the intensities compared to normal C_4H_2. It is clear that new experiments with enriched samples of diacetylene will be necessary to verify these hypotheses.

6. ^{13}C ISOTOPOLOGUES OF DIACETYLENE IN TITAN'S ATMOSPHERE

Having completed the laboratory spectroscopy and compiled a new line atlas including the ^{13}C isotopologues of diacetylene, we now added this spectral data to our existing Titan model for comparison with the observations. We had previously noted a recurring feature in Titan's spectrum as recorded by Cassini CIRS (Flasar et al. 2004) at 622.3 cm^{-1} (at 0.5 cm^{-1} resolution), that appeared to correlate with the strength of the C_4H_2 band at 628 cm^{-1}. This led us to speculate that it was due to an isotopologue of this molecule—in part the motivation for the analysis described in section 5. Having now confirmed this hypothesis, we proceeded to model the H^{13}CCCCH and HC^{13}CCCH emissions from Titan's stratosphere to measure the abundances of both isotopologues, and to thereby derive the ^{12}C/^{13}C isotopic ratio in C_4H_2 for the first time.

We selected data from CIRS observation sequences on three separate Cassini flybys of Titan (T10, T19, and T35). These are the same northern limb-view observations (instrument boresight pointed at a tangent point above the surface) analyzed in our previous study of HC_3N isotopologues (Jennings et al. 2008) except for the different spectral region modeled here (610–640 cm^{-1}). These spectral selections are highly suitable for the purpose, as both HC_3N and C_4H_2 both show similar trends in abundance, being greatly enhanced at northern latitudes at the present epoch (northern winter).

The modeling technique uses the Nemesis spectral synthesis and inversion code developed at Oxford University (Irwin et al. 2008). Compared to Jennings et al. (2008), the principal differences are (1) the new spectral atlas resulting from the laboratory study, and (2) a more realistic treatment of the spatial convolution of the detectors. Regarding this second point, only a single ray was computed to model the emission in Jennings et al. (2008), for the tangent altitude corresponding to the center of the detector's footprint on the limb, which ignores the finite projected size of the detectors. The veracity of this approximation was investigated by Nixon et al. (2009a), who showed that the approximation quickly breaks down even for relatively low signal-to-noise studies. Two improved spatial weighting models are now available, a boxcar function or a real detector response function (Nixon et al. 2009a). A follow-up study applying this spatial convolution to model low-latitude CIRS spectra of propane emission bands from Titan details the exact method used (see Section 3.2, Equations (2)–(4) of Nixon et al. 2009b).

Table 4
Retrieved Abundances for Diacetylene and ^{13}C-diacetylene (Both Isotopomers Combined)

Flyby	Date	Latitude	Q(C4H2)	Q(^{13}C-C4H2)	^{12}C/^{13}C
T10	2006 Jan 15	54°N	9.6 (0.3)	0.21 (0.04)	89 (17)
T19	2006 Oct 9	61°N	14.7 (0.4)	0.33 (0.05)	89 (14)
T35	2007 Aug 31	69°N	15.8 (0.4)	0.35 (0.05)	90 (13)
Mean					90 (8)

Note. Abundances are in ppb. Estimated uncertainties (1σ) are given in parentheses in units of the last digit quoted. The isotopic ratio has been corrected for the two-fold degeneracy in the molecular symmetry.

In Figure 4, we show the spectral data and models, averaged across all three data sets. We have included both H^{13}CCCCH and HC^{13}CCCH as a single virtual species ("^{13}C–C_4H_2") in the model with four bands, the ν_6 and ν_8 of both isotopomers centered on 622.3, 625.5, 627.1, and 627.7 cm^{-1}. The upper panel compares the data (black line) to two models: the red line showing the model with all gases and isotopes, and the green line showing the model with ^{13}C–C_4H_2 excluded (but normal C_4H_2 present). The lower panel shows the (data-model) residual, emphasizing that without the inclusion of the isotopologues of C_4H_2, two peaks of residual emission at 622.3 and 627.5 (blended ν_8 bands) remain. Due to the spectral resolution of CIRS (0.5 cm^{-1}) we cannot actually resolve the bands near 627.5 cm^{-1} from each other, or from the main emission at 628 cm^{-1}, therefore the abundance of ^{13}C–C_4H_2 is actually constrained by the isolated feature at 622.3 cm^{-1}. For this band, we find an emission of 11.4 nW cm^{-2} sr^{-1} cm^{-1} corresponding to a detection significance of 3.3σ (where 1σ is the instrumental NESR = noise equivalent spectral radiance).

Table 4 gives the numerical results of the abundance determinations at each latitude, for both the ^{12}C and ^{13}C-substituted isotopomer, and also the implied isotopic ratio ^{12}C/^{13}C. Our abundances for C_4H_2, which apply to 150 km altitude approximately (2 mbar), agree well with previous investigations of the CIRS data set (Teanby et al. 2008a, 2009a; Vinatier et al. 2010), showing the well-known increasing abundance at northern latitudes above 40°N due to the enriched air of the north polar vortex (at this epoch). See Teanby et al. (2008b, 2009b) for further details and discussion of the dynamical implications. For the first time on Titan, we are able here to provide abundances for ^{13}C–C_4H_2 and its carbon isotopic ratio. The individual values for ^{12}C/^{13}C at all three latitudes measured independently are in extremely good agreement, and the weighted mean value is 90 ± 8.

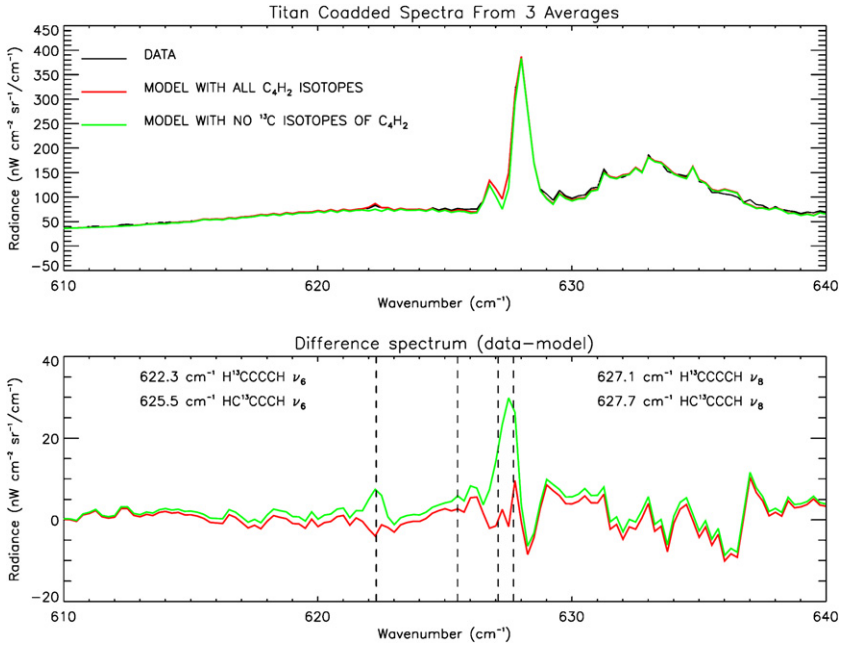

Figure 4. Upper: mean observed spectrum of Titan from averaged data set presented in Table 4 compared to model spectra with and without the contribution of ^{13}C isotopologues of C_4H_2. Lower: residual emission obtained after subtracting the observed spectrum and both model spectra.
(A color version of this figure is available in the online journal.)

Previously, the stable carbon isotopic ratio has been measured by CIRS in a variety of Titan molecules (see the previous section). Notably, the measured $^{12}C/^{13}C$ in methane as measured by both CIRS (76 ± 3) and the Huygens probe GCMS mass spectrometer (82 ± 1) show a definite enrichment in ^{13}C in methane relative to the telluric reference value (89.4). This terrestrial standard however appears compatible with the mean value for giant planet atmospheres (88 ± 7; Sada et al. 1996). Titan's other molecules (HCN, C_2H_2, C_2H_6, CO_2, HC_3N) show $^{12}C/^{13}C$ in the range 75–90, mostly with error bars that are sufficiently large to encompass both the terrestrial (89) and Titan methane (∼80) values, so that it is difficult to ascertain whether there is real differentiation in the ratio in different Titan molecules.

The exception is ethane, for which the CIRS result has recently been combined with ground-based spectroscopic measurements to place a tighter limit of 89.4 ± 5.8, that is compatible with the terrestrial value but not the Titan methane value (Jennings et al. 2009). The authors of this study have proposed an explanation, via a difference in reaction rates of $^{12}CH_4$ and $^{13}CH_4$ in the abstraction of H from methane by the ethynyl radical C_2H, which creates CH_3 that is a precursor to ethane. This phenomenon, known as the *kinetic isotope effect* (KIE) is quantified as the ratio of the reaction rates in the two cases. A plausible KIE of 1.08 is sufficient to explain how atmospheric methane could become enriched in ^{13}C relative to an incoming flux of terrestrial-ratio methane from a reservoir, which is required to replace the steady, irreversible depletion of CH_4 in the atmosphere.

The $^{12}C/^{13}C$ that we have determined for diacetylene is in good agreement with the terrestrial value, and also compatible with that measured for acetylene (85 ± 3) by CIRS as we would expect, because once the triple covalent bond is formed it should tend to persist. We are also in agreement with the less accurate value for HC_3N (79 ± 17). Further work is required to refine these values, which should be possible through more sensitive observations planned for the *Cassini* Solstice Mission (2010–2017).

7. CONCLUSION

Experimental spectra of diacetylene at low temperature were recorded to sort out the difficult problem of the numerous hot bands accompanying the ν_8 fundamental transitions. Because of the complexity of the rovibrational energies of C_4H_2, it was necessary to develop a global analysis on the basis of high-resolution spectra, some of them available in the literature, but most of them specially recorded by Levi-Matti Horneman in Oulu. More than 400 subbands were fitted, most of them assigned for the first time, giving a coherent set of molecular parameters for C_4H_2 from which a calculated spectrum was generated to obtain a new extended line list which could be validated through a comparison with both room and low-temperature spectra. In addition, the positions and the intensities of the ν_6 and ν_8 bands of both ^{13}C isotopomers of diacetylene have been established for the first time, thanks to the low resolution spectra and the ab initio isotopic shifts recently published by Simmonett et al. (2009).

Finally, recent observational data from Titan's atmosphere obtained by the *Cassini* mission were analyzed using the new line list of diacetylene and its ^{13}C-isotopologues. The result was an important improvement in the fit of the ν_8 band of diacetylene and a clear detection of both $H^{13}CCCCH$ and $HC^{13}CCCH$ which are observed in Titan for the first time. A new $^{12}C/^{13}C$ isotopic ratio could be determined in very good agreement with previous determinations.

A.F. thanks Eric Arié for the original spectra of the ν_9 and ν_8 bands and he expresses his gratitude to Veli-Matti Horneman who kindly agreed to synthesize the diacetylene sample and to record new spectra over a quite broad range. C.A.N. and D.E.J. acknowledge the support of the NASA *Cassini* Data Analysis Program Grant NNX09AK55G, and

the *Cassini* Flagship Mission. A.J. and Y.B. acknowledge the support of the Programme National de Planétologie (PNP) and CNES.

REFERENCES

Amyay, B., et al. 2009, J. Chem. Phys., 131, 14
Arié, E., & Johns, J. W. C. 1992, J. Mol. Spectrosc., 155, 195
Bernard-Salas, J., Peeters, E., Sloan, G. C., Cami, J., Guiles, S., & Houck, J. R. 2006, ApJ, 652, L29
Bezard, B., Nixon, C. A., Kleiner, I., & Jennings, D. E. 2007, Icarus, 191, 397
Botschwina, P. 1982, Mol. Phys., 47, 241
Burgdorf, M., Orton, G., van Cleve, J., Meadows, V., & Houck, J. 2006, Icarus, 184, 634
Cernicharo, J., Heras, A. M., Tielens, A. G. G. M., Pardo, J. R., Herpin, F., Guélin, M., & Waters, L. B. F.M. 2001, ApJ, 546, L123
Coustenis, A., & Bezard, B. 1995, Icarus, 115, 126
Coustenis, A., Bezard, B., & Gautier, D. 1989, Icarus., 80, 54
Coustenis, A., Salama, A., Schulz, B., Ott, S., Lellouch, E., Encrenaz, T., Gautier, D., & Feuchtgruber, H. 2003, Icarus, 161, 383
Coustenis, A., et al. 2008, Icarus, 197, 539
de Graauw, Th., et al. 1997, A&A, 321, L13
Fayt, A., Vigouroux, C., & Winther, F. 2004, J. Mol. Spectrosc., 224, 114
Fayt, A., Willaert, F., Demaison, J., Starck, T., Mader, H., Pawelke, G., Mkadmi, E. B., & Burger, H. 2008, Chem. Phys., 346, 115
Flasar, M., et al. 2004, Space Sci. Rev., 115, 169
Guelachvili, G., Craig, A. M., & Ramsay, D. A. 1984, J. Mol. Spectrosc., 105, 156
Hardwick, J. L., Ramsay, D. A., Garneau, J. M., Lavigne, J., & Cabana, A. 1979, J. Mol. Spectrosc., 76, 492
Irwin, P. G. J., et al. 2008, J. Quant. Spectrosc. Radiat. Transfer, 109, 1136
Jacquinet-Husson, N., et al. 2005, J. Quant. Spectrosc. Radiat. Transfer, 95, 429
Jennings, D. E., et al. 2008, ApJ, 681, L109
Jennings, D. E., et al. 2009, J. Phys. Chem. A., 113, 11101
Jolly, A., & Benilan, Y. 2008, J. Quant. Spectrosc. Radiat. Transfer, 109, 963
Jolly, A., Benilan, Y., & Fayt, A. 2007, J. Mol. Spectrosc., 242, 46
Khlifi, M., Paillous, P., Delpech, C., Nishio, M., Bruston, P., & Raulin, F. 1995, J. Mol. Spectrosc., 174, 116
Khlifi, M., Raulin, F., & Dang-Nhu, M. 1992, J. Mol. Spec., 155, 77
Koops, T., Visser, T., & Smit, W. M. A. 1984, J. Molec. Struct., 125, 179
Kunde, V. G., Aikin, A. C., Hanel, R. A., Jennings, D. E., Maguire, W. C., & Samuelson, R. E. 1981, Nature, 292, 686
Kunde, V. G., et al. 2004, Science, 305, 1582
Matsumura, K., Etoh, T., & Tanaka, T. 1981, J. Mol. Spectrosc., 90, 106
Matsumura, K., Kawaguchi, K., Hirota, E., & Tanaka, T. 1986, J. Mol. Spectrosc., 118, 530
Matsumura, K., & Tanaka, T. 1982, J. Mol. Spectrosc., 96, 219
Meadows, V. S., Orton, G., Line, M., Liang, M. C., Yung, Y. L., Van Cleve, J., & Burgdorf, M. J. 2008, Icarus, 197, 585
Nixon, C. A., et al. 2008a, Icarus, 195, 778
Nixon, C. A., et al. 2008b, ApJ, 681, L101
Nixon, C. A., et al. 2009a, Appl. Optics, 48, 1912
Nixon, C. A., et al. 2009b, Planet. Space Sci., 57, 1573
Sada, P. V., McCabe, G. H., Bjoraker, G. L., Jennings, D. E., & Reuter, D. C. 1996, ApJ, 472, 903
Simmonett, A. C., Schaefer, H. F., & Allen, W. D. 2009, J. Chem. Phys., 130, 10
Tay, R., Metha, G. F., Shanks, F., & McNaughton, D. 1995, Struct. Chem., 6, 47
Teanby, N. A., Irwin, P. G. J., de Kok, R., Jolly, A., Bezard, B., Nixon, C. A., & Calcutt, S. B. 2009a, Icarus, 202, 620
Teanby, N. A., Irwin, P. G. J., de Kok, R., & Nixon, C. A. 2009b, Phil. Trans. R. Soc., A 367, 697
Teanby, N. A., et al. 2008a, Icarus, 193, 595
Teanby, N. A., et al. 2008b, J. Geophys. Res. Planets, 113, 13
Vinatier, S., Bezard, B., & Nixon, C. A. 2007a, Icarus, 191, 712
Vinatier, S., et al. 2007b, Icarus, 188, 120
Vinatier, S., et al. 2010, Icarus, 205, 559
Winther, F. 1973, Z. Naturforsch. A, 28, 1179
Winther, F., Horneman, V. M., Vigouroux, C., & Fayt, A. 2005, J. Mol. Struct., 742, 131